Ginzburg-Landau theory of ternary amphiphilic systems. II. Monte Carlo simulations

G. Gompper and Martin Kraus
Sektion Physik der Ludwig-Maximilians Universität München, Theresienstrasse 37, 8000 München 2, Germany
(Received 7 January 1993)

We study interfacial fluctuations in a Ginzburg-Landau model for ternary oil-water-surfactant mixtures by Monte Carlo simulations. Space has to be discretized in order to apply the Monte Carlo method. However, by an appropriate choice of the lattice constant of the background lattice, discretization effects can be largely avoided. Strong fluctuation effects on the phase diagram are observed, which can be explained by a fluctuation-induced lowering of the oil-water interfacial tension. We determine several quantities, which characterize the structure of the microemulsion, such as the internal interfacial area and the Euler characteristic. The microemulsion phase is shown to have a disordered bicontinuous structure. In the lamellar phase, we observe an increase of the interfacial area with increasing separation of the monolayers. A quantitative comparison with the predictions of the effective curvature model of Helfrich [J. Phys. (Paris) **46**, 1263 (1985)] yields excellent agreement, when an exponential distance dependence of the interfacial tension is taken into account.
PACS number(s): 82.70.−y, 61.20.Gy, 05.40.+j

I. INTRODUCTION

The reduction of the interfacial tension between oil and water by a small amount of amphiphile is responsible for a large number of interesting phenomena in ternary amphiphilic systems [1]. For medium- and long-chain amphiphiles, phases with a large amount of internal oil-water interface are possible. Two phases are of particular importance in balanced systems: the lamellar phase, a one-dimensional stack of oil and water films, separated by amphiphilic monolayers, and the microemulsion, a random array of monolayers separating two intertwined networks of oil and water channels [2, 3]. Due to the low or vanishing interfacial tensions, fluctuations of the monolayers are controled by the bending energy in these systems [4]. The fluctuations lead to an entropic repulsion of the monolayers [5], and thus to a swelling of the lamellar phase. For small bending rigidity, fluctuations destroy the lamellar order and stabilize the microemulsion [6].

In this paper we want to study these fluctuation effects in a Ginzburg-Landau theory of ternary amphiphilic mixtures. We have studied interface fluctuations in this model by the Gaussian approximation in the first paper of this series [7]. However, this approximation works best for small fluctuations, a condition which is not necessarily satisfied in a system with small interfacial tensions. Thus, we use Monte Carlo simulations in this work, a method well suited for systems with large fluctuations. Monte Carlo simulations have already been used to study various lattice models [8] of ternary amphiphilic systems [9–12]. The advantage of the Ginzburg-Landau model is that it is defined in the continuum. In a computer simulation, it is of course necessary to discretize space, but now the lattice constant a has no physical meaning. By choosing a sufficiently small value for a, lattice effects can be largely avoided in the simulations [13]. This is very important for all properties where the scale invariance of the curvature energy is relevant.

The continuum Ginzburg-Landau model, as well as its discretized version, are introduced in Sec. II. We show for an exactly soluble case that the correlation functions calculated by the Monte Carlo method for the discretized model agree quite well with the continuum correlation functions. In Sec. III, we determine the effect of fluctuations on the phase diagram. We find that the fluctuations stabilize the lamellar phase and the microemulsion. The structure of the microemulsion is studied in Sec. IV. Here, Monte Carlo simulations give a much more detailed picture of the microemulsion phase than all other methods. In particular, we can study the topology of this phase by calculating its Euler characteristic. The fluctuations in the lamellar phase are investigated in Sec. V. We focus our attention on the change of the interfacial area with the lamellar spacing. For a quantitative comparison with the predictions of Helfrich's curvature model, a distance-dependent interfacial tension [7, 14] has to be taken into account. We are then able to show that our Ginzburg-Landau results are consistent with the logarithmic increase of the interfacial area with increasing distance between interfaces as predicted by Helfrich [15].

II. GINZBURG-LANDAU MODEL

Our analysis is based on the free-energy functional [16]

$$\mathcal{F}\{\Phi\} = \int d^3r \ \left[c(\Delta\Phi)^2 + g(\Phi)(\nabla\Phi)^2 + f(\Phi) - \mu\Phi\right] \tag{1}$$

for a scalar order-parameter field $\Phi(\mathbf{r})$, which is proportional to the local difference of the oil and water concentrations. Here, μ is the chemical potential difference between oil and water. The amphiphile degrees of freedom are considered as being integrated out in this ap-

proach [17]. The properties of the amphiphile and its concentration enter the theory via the form of the functions f and g, as well as the magnitude of the constant c. In the absence of amphiphilic molecules, $f(\Phi)$ has two minima at $\Phi = \Phi_o$ and $\Phi = \Phi_w$, which describe the oil and water phases, and $g(\Phi)$ is a positive constant. When amphiphile is added to the system, a third minimum of f appears at $\Phi = 0$, which describes the homogeneous microemulsion phase. Simultaneously, a minimum of g develops at $\Phi = 0$. For strong amphiphiles $g(\Phi)$ becomes negative in the microemulsion phase; this leads to a scattering peak at nonzero wave vector q as observed in many neutron-scattering experiments [18].

We expand f and g in a power series in Φ, so that we arrive at a Ginzburg-Landau theory with

$$f(\Phi) = \omega(\Phi - \Phi_o)^2(\Phi^2 + f_0)(\Phi - \Phi_w)^2,$$
$$g(\Phi) = g_0 + g_2\Phi^2 \ . \tag{2}$$

In this paper we choose

$$g_2 = 4\sqrt{1 + f_0} - g_0 + 0.01, \tag{3}$$

which ensures that the correlation function in the oil-rich and the water-rich phases decays monotonically.

We will focus here on systems with oil-water symmetry, so that $-\Phi_o = \Phi_w \equiv \Phi_{\text{bulk}} = 1$, and $\mu = 0$. The other parameters are taken to be $c = 1$ and $\omega = 1$. Phase diagrams are then calculated in the parameters f_0 (measuring the deviation from oil-water-microemulsion coexistence) and g_0 (proportional to the chain length of the amphiphile [19]). The mean-field phase diagram [20] (which is obtained by minimizing the free-energy functional $\mathcal{F}$) for this model is shown in Fig. 1. In addition to the three homogeneous phases, oil, water, and microemulsion, a lamellar phase appears at large enough negative g_0.

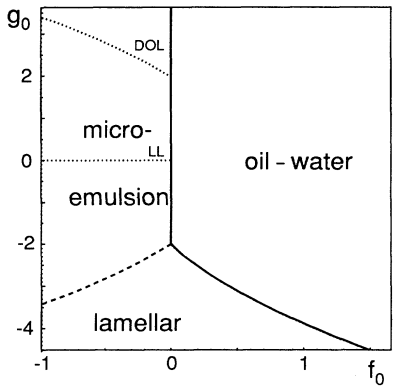

FIG. 1. Mean-field phase diagram of the Ginzburg-Landau model (1). Full lines are first-order transitions, dashed lines are second-order transitions. In the microemulsion phase, the Lifshitz line (LL), where the scattering intensity loses its peak at $q > 0$, and the disorder line (DOL), where the oscillations in the correlation function vanish, are indicated by dotted lines. The transition from oil-water coexistence to the lamellar phase is indistinguishable from the $\sigma = 0$ line of a free oil-water interface, obtained from approximation (A6).

A. Discretized Ginzburg-Landau model

A Monte Carlo simulation of the continuum model is not possible. We therefore have to discretize space. This is done by introducing a cubic $N \times N \times N$ lattice (lattice constant a) with periodic boundary conditions. However, the order parameter itself is kept as a continuous variable, which can take any real value. A Monte Carlo step then consists of an attempt to update the order parameter on each lattice site in sequence by a random increment in the interval $[-s, s]$. The maximal increment s is chosen such that about 50% of the updating attempts are accepted.

The potential term $f(\Phi)$ remains unchanged by the discretization. The gradient term becomes

$$\int d^3r\ g(\Phi)(\nabla\Phi)^2 \longrightarrow \sum_{\langle i,j\rangle} g(\tfrac{1}{2}[\Phi(\mathbf{r}_i) + \Phi(\mathbf{r}_j)]) \times \left(\frac{\Phi(\mathbf{r}_i) - \Phi(\mathbf{r}_j)}{a}\right)^2, \tag{4}$$

where $\langle i,j\rangle$ denotes the sum over pairs of nearest neighbors. Finally, the Laplacian term takes the form

$$\int d^3r\ c(\Delta\Phi)^2 \longrightarrow c\sum_i \left(\sum_{k=1}^{3} \frac{\Phi(\mathbf{r}_i + \mathbf{e}_k) - 2\Phi(\mathbf{r}_i) + \Phi(\mathbf{r}_i - \mathbf{e}_k)}{a^2}\right)^2 \tag{5}$$

where the $\mathbf{e}_k$ are the three basic lattice vectors.

The lattice constant a is an additional parameter in the discretized model. We want to choose the lattice constant such that (i) a is (much) smaller than all other characteristic length scales, in particular the correlation lengths in the bulk phases and the width of the oil-water interface, in order to minimize lattice effects; (ii) the overall system size Na is (much) larger than the correlation lengths of the bulk phases, in order to avoid finite-size effects. Obviously these requirements are contradictory and require some compromise for given lattice size N. However, we will see in Sec. II B that we are able to satisfy both conditions with reasonable lattice sizes.

B. Simulation of the Gaussian Model

A special case of our model is the Gaussian model, originally studied by Teubner and Strey [18] to describe the scattering behavior of microemulsions. In this case we have $f(\Phi) = \omega\Phi^2$ and $g(\Phi) = g_0$ =const. This model can be solved exactly, both in the continuum and on the lattice. It therefore serves as a test of the importance of lattice and finite-size effects, and for the statistical accuracy of the Monte Carlo data.

The correlation function in the Fourier space of the

continuum system is given exactly by

$$(G(q))^{-1} = \omega + g_0 q^2 + c q^4 \ . \tag{6}$$

For the lattice system, we have

$$(G(\mathbf{q}))^{-1} = \omega + g_0 Q(\mathbf{q})^2 + c Q(\mathbf{q})^4 \ , \tag{7}$$

where

$$Q(\mathbf{q})^2 \equiv \frac{1}{a^2}\left[6 - 2\cos(q_x a) - 2\cos(q_y a) - 2\cos(q_z a)\right] \ . \tag{8}$$

To compare with the simulation results, we need the correlation function in real space,

$$G(\mathbf{r}) = \sum_{\mathbf{q}} e^{i\mathbf{q}\cdot\mathbf{r}} G(\mathbf{q}) \ , \tag{9}$$

where the sum is over all reciprocal-lattice vectors. With (7), it is also possible to calculate the energy density,

$$\frac{\langle \mathcal{F}\{\Phi\}\rangle}{V} = \frac{1}{2a^3} \ . \tag{10}$$

The results for the correlation function $G(r)$ in three different directions of high symmetry in the cubic lattice are shown in Fig. 2 for lattice constant $a = 0.8$ and $N = 27$. It can be seen that the agreement between the different directions is very good until the correlation functions begin to be affected by the periodic boundary conditions. Furthermore, the data also agree with the continuum correlation function very well. Thus, we are confident that with this choice of parameters lattice effects are small.

III. PHASE DIAGRAM OF TERNARY AMPHIPHILIC SYSTEMS

We now want to determine the phase diagram of the model (1), (2) for ternary amphiphilic mixtures. For the calculation of thermal averages, we usually take averages over 25 000 to 150 000 Monte Carlo steps per site (MCS), with the longer runs in the vicinity of the phase transitions. The Monte Carlo phase diagram is shown in Fig. 3. The phase transition between the microemulsion and the lamellar phase is found to be very weakly first order (see Sec. III C for details), so that its location could be determined easily. The transitions from oil-water coexistence to both the microemulsion and the lamellar phase, however, are strongly first order; in this case, hysteresis effects make a precise determination of the transition line difficult. We have located the transitions by determining the limits of metastability of oil-rich, water-rich, and microemulsion phases.

A. Renormalization of the interfacial tension

A comparison of the Monte Carlo and the mean-field phase diagrams, Figs. 1 and 3, shows that the region of stability of the microemulsion increases due to the fluctuations, both towards the oil-water coexistence and the lamellar phase. Also the lamellar phase extends into regions where the oil-rich or water-rich phases are stable in mean-field theory. Thus, we find that the fluctuations stabilize phases with an extensive amount of internal interface, as expected.

We can understand the shift of the transition lines by studying the renormalization of the interfacial tension due to the fluctuations. The transition from oil-water coexistence to a phase with internal interfaces should occur in close vicinity to the line where the renormalized tension vanishes. For small displacements $u(\mathbf{x})$ from a flat reference state, we use the effective curvature Hamiltonian [4, 21]

$$\mathcal{H}_{\rm curv}\{u\} = \int d^2x \ \{\sigma_0[1 + \tfrac{1}{2}(\nabla u)^2] + \tfrac{1}{2}\kappa(\Delta u)^2\}. \tag{11}$$

The renormalized tension is the free energy per unit area,

$$\sigma = -\frac{1}{(Na)^2} \ln\left[\lambda^{N^2} \int \mathcal{D}u \ e^{-\mathcal{H}_{\rm curv}\{u\}}\right] \ , \tag{12}$$

where λ is a constant which makes the argument of the logarithm dimensionless. With the quadratic approxima-

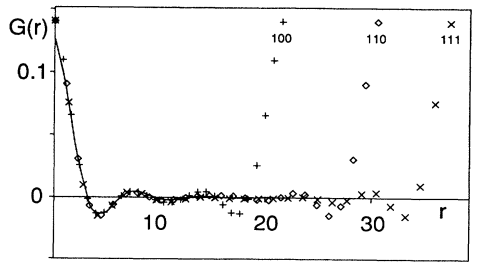

FIG. 2. Correlation function $G(r) = \langle \Phi(0)\Phi(r)\rangle$ of the Gaussian model on the lattice for $g_0 = -1.9$, $c = \omega = 1$ with $a = 0.8$, $N = 27$, the values used for most simulations. Data are plotted for three directions of high symmetry in the cubic lattice. The solid line is the correlation function $G(r)$ for the infinite continuum system.

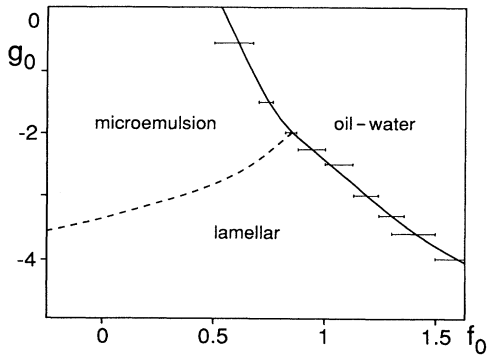

FIG. 3. Phase diagram as obtained from the Monte Carlo simulations. Error bars denote regions where metastable phases occur; see discussion in the text. The dashed line indicates a weakly first-order transition.

tion (11) this is again a Gaussian functional integral. A simple calculation in Fourier space yields

$$\sigma_R = \sigma_0 - \sum_{\mathbf{q}} \ln \frac{Na\lambda}{\sqrt{2\sigma_0 q^2 + 2\kappa q^4}} . \tag{13}$$

This expression is evaluated by summing over the reciprocal-lattice vectors of a two-dimensional $N \times N$ square lattice. The result obviously depends on the value of the parameter λ [22]. λ has the dimension of an inverse volume. We obtain the best agreement with the Monte Carlo results when we take λ to be of order a^{-3}. The resulting renormalized interfacial tension is shown in Fig. 4(a). The line $\sigma_R = 0$ reproduces the shape of the line of phase transition to oil-water coexistence quite well.

Similarly, the phase transition from the microemulsion to the lamellar phase can be understood by studying the bending rigidity κ of the interfaces. In this case, renormalization effects [23,15] are not important, because they only change κ by an additive constant. The bending rigidity κ, calculated within the mean-field approximation (see Appendix A), is shown in Fig. 4(b). The line $\kappa = 2.5$ describes the shape of the transition line reasonably well [24]. This behavior agrees with results obtained from the curvature model [4], where the transition is expected to occur when the persistence length ξ_K is of the order of the lamellar spacing [6]. Since $\xi_K \sim \exp(c\kappa)$, with a constant c of order 1, this is equivalent to a transition at constant bending rigidity κ.

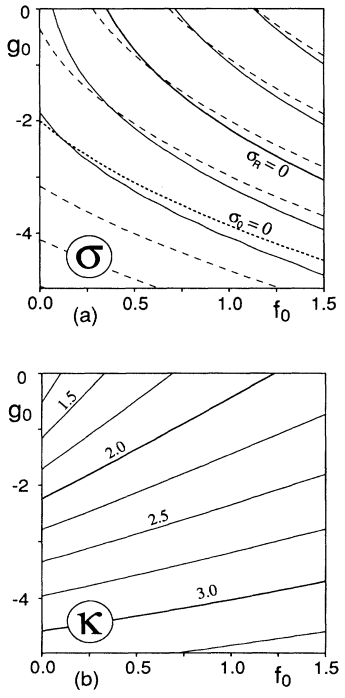

FIG. 4. (a) Contour plot of the interfacial tension of a free oil-water interface. Dashed lines are the mean-field results, solid lines give the interfacial free energy with capillary-wave contributions included. Here, the parameter $\lambda = (0.45)^{-3}$ is used in (12). (b) Contour plot of the bending rigidity of the oil-water interface in mean-field approximation; details of the calculation are given in Appendix A.

B. The phase-transition microemulsion–oil-water

We now want to study the transition from the microemulsion to oil-water coexistence in more detail. In Figs. 5(a) and 5(b), we present data as a function of f_0, for $g_0 = -1.5$. In all figures the existence of metastable states is clearly visible. The internal energy $U = \langle \mathcal{F} \rangle$ and the specific heat $C = \langle \mathcal{F}^2 \rangle - \langle \mathcal{F} \rangle^2$ are shown in Fig. 5(a). The internal energy U increases roughly linearly with f_0 in the microemulsion phase, as expected from the form of the potential $f(\Phi)$, and is roughly constant in the oil or water phase. The specific heat shows a strong peak in the metastable region, which is an indication for the position of the first-order transition.

More interesting in the context of amphiphilic systems is the area of internal interfaces, as well as the magnitude of the order-parameter fluctuations, shown in Fig. 5(b). Since Φ is proportional to the concentration difference of oil and water, we define the internal interface as the

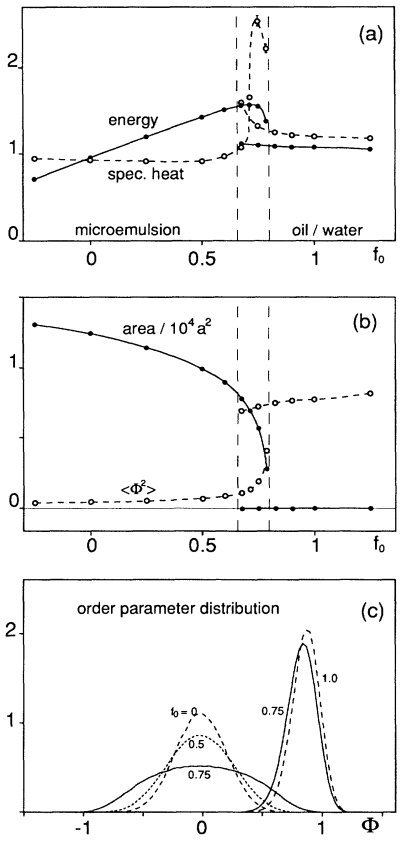

FIG. 5. Phase transition from microemulsion to oil-water coexistence at $g_0 = -1.5$. (a) Internal energy and specific heat, (b) internal area and order-parameter variation, and (c) order-parameter distribution function (not normalized). Dashed lines indicate the width of the metastable region.

$\Phi(\mathbf{r}) = 0$ surface. A few details about the calculation of the internal area in the simulations are given in Appendix B. In the oil and water phases, the internal area vanishes (or is extremely small), whereas the internal area increases rapidly in the microemulsion phase with decreasing f_0. The fluctuations of the order parameter, $\langle\Phi^2\rangle$, and the order-parameter distribution shown in Fig. 5(c), give additional information about the structure of the microemulsion: in the vicinity of the phase transition, the order-parameter distribution in the microemulsion becomes very broad, indicating that the system contains large oil-rich and water-rich regions.

C. The phase-transition microemulsion–lamellar phase

Data for the transition from the microemulsion to the lamellar phase are shown in Figs. 6(a) and 6(b) for $g_0 = -2.5$, again as a function of f_0. The behavior of all thermal averages shown in these figures indicates that this transition is very weakly first order, while it was found to be second order in the mean-field approximation. Hysteresis effects have not been observed. The transition to a lamellar phase is indeed expected to be fluctuation-induced first order [25]. However, we want to emphasize that in our simulation the periodicity of the lamellar phase is restricted by the periodic boundary conditions and the fixed system size to take a small number of discrete values. The order of the transition could be different when the periodicity of the lamellar phase is allowed to vary continuously.

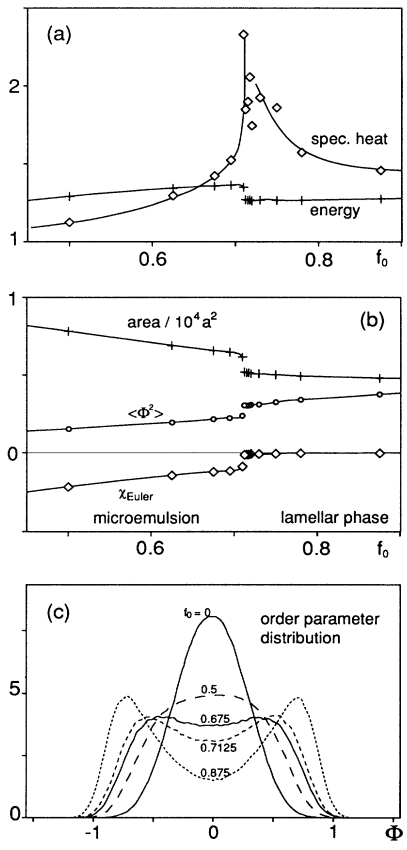

FIG. 6. Phase transition from microemulsion to the lamellar phase at $g_0 = -2.5$. (a) Internal energy and specific heat, (b) internal area, order-parameter variation, and Euler characteristic, an (c) order-parameter distribution function (not normalized).

The energy again increases approximately linearly in the microemulsion, and is roughly independent of f_0 in the lamellar phase, see Fig. 6(a). The peak in the specific heat signals the position of the phase transition. The fluctuations of the order parameter, $\langle\Phi^2\rangle$, increase strongly on the microemulsion side of the transition, as shown in Fig. 5(b) and Fig. 6(b). Simultanously, the area decreases; see Fig. 6(b). The behavior of the internal area in the lamellar phase will be studied in more detail in Sec. V. The topology of the microemulsion can be characterized by the Euler characteristic χ_E [26]. We calculate this topological invariant by using a lattice formulation [27], in which plaquettes between lattice sites with different order-parameter signs are interpreted as pieces of internal interface. The Euler characteristic is strongly negative in the microemulsion; this indicates a phase with multiply connected oil and water channels, as expected for a bicontinuous structure. As the transition is approached, χ_E decreases in magnitude, i.e., the characteristic length scale of the bicontinuous structure increases.

D. The phase-transition lamellar phase–oil-water

The phase transition from oil-water coexistence to the lamellar phase is a first-order transition in the mean-field approximation. When fluctuations are taken into account, a continuous unbinding transition is expected to occur, if the fluctuations are dominated by the bending energy and the interactions are sufficiently short ranged [28]. Both conditions are fulfilled in our system. However, such a continuous unbinding transition cannot be observed in our simulations, due to the restriction to a discrete number of layers, as discussed in Sec. III C above.

We find that lamellar states on the oil-water side of the transition, where the interfacial tension is positive, are extremely long lived. Therefore, in the phase diagram, Fig. 3, we have plotted the line were the homogeneous water phase becomes unstable with respect to the lamellar phase in very long runs (typically 10^5 MCS). A better determination of the transition line requires a considerably larger effort.

IV. MICROEMULSION STRUCTURE

From the results presented in Sec. III, it can already be seen that the simulations yield structural information on the microemulsion phase going considerably beyond what can be extracted from the mean-field and Ornstein-Zernike approximations. The most interesting part of the phase diagram is certainly the region near four-phase co-

existence, where the microemulsion is characterized by large order-parameter fluctuations, which we interpret as coherent oil and water regions, which are separated by amphiphilic monolayers. In the region $f_0 \leq 0$, on the other hand, where the microemulsion is stable in mean-field theory, the fluctuations are much smaller, as is the typical length scale of homogeneous regions. Therefore, we focus our attention on $f_0 > 0$ and $g_0 < 0$. Typical configurations of the microemulsion phase are shown in Fig. 7. A cut through this structure strongly resembles the pictures of microemulsion structure obtained experimentally by freeze-fracture microscopy [29].

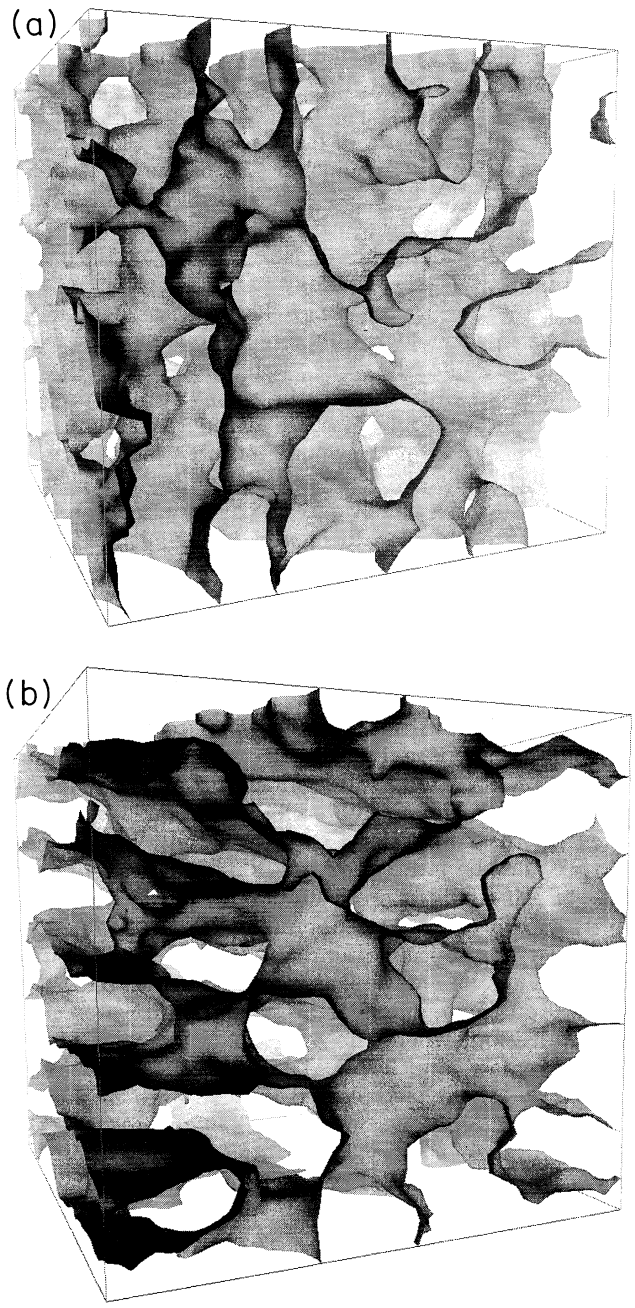

FIG. 7. Typical equilibrium configurations in the microemulsion in the vicinity of the transition to the lamellar phase at (a) $g_0 = -2.5, f_0 = 0.675$ and (b) $g_0 = -2.5, f_0 = 0.695$. Shown are only the $\Phi(\mathbf{r}) = 0$ surfaces. It can be seen that (b) is closer to the transition line, and shows already a local lamellar structure.

A. Structure factor and typical length scales

The structure factor of the Ginzburg-Landau model calculated from the Monte Carlo simulations will certainly be different from the Ornstein-Zernike result [30]. Nevertheless, the expansion of the scattering intensity for small wave vector q to fourth order in q is still possible,

$$S(q) = \frac{S(0)}{1 + \tilde{b}q^2 + \tilde{c}q^4} \tag{14}$$

and turns out to be a convenient way to describe the behavior of the scattering intensity near its maximum, $q^* = \sqrt{-\tilde{b}/2\tilde{c}}$, just as in experiment [18, 31]. By Fourier transform of the scattering intensity (14) the correlation length ξ and the characteristic wave vector k of the asymptotic decay of the correlation function can be extracted [18],

$$\xi = \left(\frac{1}{2}\frac{1}{\sqrt{\tilde{c}}} + \frac{1}{4}\frac{\tilde{b}}{\tilde{c}}\right)^{-1/2}, \tag{15}$$

$$k = \left(\frac{1}{2}\frac{1}{\sqrt{\tilde{c}}} - \frac{1}{4}\frac{\tilde{b}}{\tilde{c}}\right)^{+1/2}. \tag{16}$$

We find that the correlation length ξ increases in the vicinity of four-phase coexistence, and decreases with decreasing quality of the amphiphile (increasing g_0). The characteristic wave vector k increases with increasing distance from oil-water coexistence, just as in the lamellar phase. An important dimensionless quantity is the product $k\xi$. With $\tilde{b}_{\rm DO} = 2\sqrt{\tilde{c}\,[S(0)]^{-1}}$, the value of $\tilde{b}$ at the disorder line, it reads

$$k\xi = \sqrt{\frac{1 - \tilde{b}/\tilde{b}_{\rm DO}}{1 + \tilde{b}/\tilde{b}_{\rm DO}}}. \tag{17}$$

In the limit $\tilde{b} \to -\tilde{b}_{\rm DO}$, $k\xi$ diverges. For $\tilde{b} \to 0$, one finds $q^* \to 0$ and $k\xi \to 1$. The results for $k\xi$ and q^* obtained from the simulation are shown in Figs. 8(a) and 8(b), respectively. A maximum of $k\xi$ is found to occur at four-phase coexistence, just as in the Ornstein-Zernike approximation.

Our values of $k\xi$ can be compared with experimental results. An analysis of scattering data for different amphiphilic systems [18, 31, 32] gives values for $k\xi$ in the range from 1.67 to 4.77, with higher values for systems with large amphiphile concentrations, i.e., near the lamellar phase. This is in good agreement with the results presented in Fig. 8(a).

B. Topology, internal area, and bicontinuity

We have seen in Sec. III C that the microemulsion can also be characterized by its internal area A and its Eu-

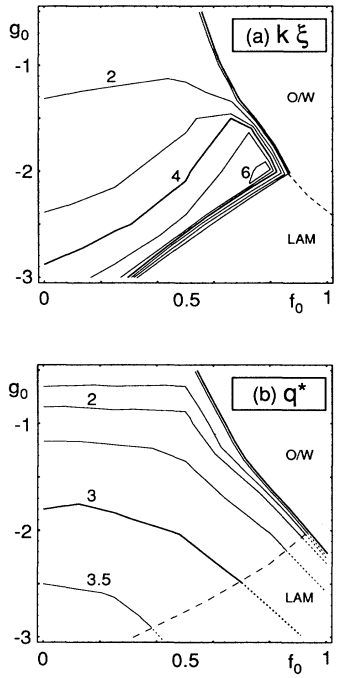

FIG. 8. Quantities characterizing the shape of the microemulsion structure factor: (a) the dimensionless product $k\xi$, which is the ratio of the two length scales in the correlation function, (b) the peak position q^* in units of $2\pi/(\mathrm{Na})$. The dashed lines indicate the positions of the phase transitions; compare Fig. 3.

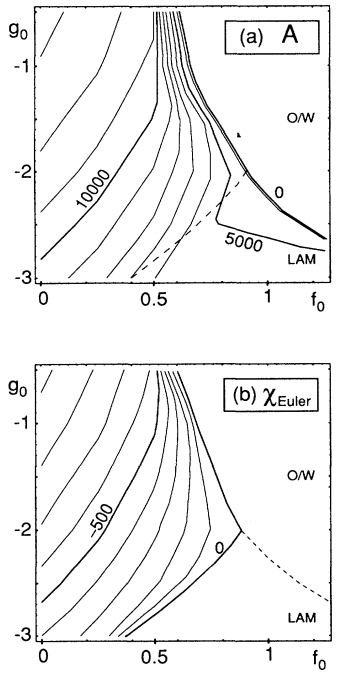

FIG. 9. Quantities characterizing the structure of the microemulsion: (a) area A of internal oil-water interface, (b) Euler characteristic χ_E. The dashed lines indicate the positions of the phase transitions; compare Fig. 3.

ler characteristic χ_E. Contour plots of A and χ_E are shown in Figs. 9(a) and 9(b), respectively. We have already noted that the negative Euler characteristic in the microemulsion phase indicates a bicontinuous structure with multiply connected labyrinths of oil-rich and water-rich regions. This conclusion is confirmed by an analysis of the cluster statistics, where two large clusters contain almost all sites. The internal area increases with decreasing quality of the amphiphile (increasing distance from the transition to the lamellar phase), i.e., the size of coherent oil and water regions decreases. This behavior, however, indicates that the internal area cannot simply be proportional to the amphiphile concentration, since in experimental systems the amphiphile concentration in the lamellar phase is larger than the concentration in the microemulsion; such a proportionality would also contradict our conclusions drawn from the behavior of $k\xi$ in Sec. IV A. Thus, for weak amphiphiles the internal interface can only be covered partially by a layer of amphiphiles.

In a bicontinuous structure, the area and the Euler characteristic are not independent. Let us assume that the microemulsion of total volume $V = L^3$ is composed of building blocks of typical length scale L_0. All these elementary units have approximately the same structure and topology, with a typical Euler characteristic χ_0, which is independent of L_0. Then, the Euler characteristic of the whole system is

$$\chi_E(V) = \chi_0 \left(\frac{L}{L_0}\right)^3 . \tag{18}$$

The internal area of the elementary unit is $A(V_0) = \tilde{A} L_0^2$, so that the area of the whole system is given by

$$A(V) = \tilde{A} L_0^2 \left(\frac{L}{L_0}\right)^3 = \tilde{A} V^{2/3} \frac{L}{L_0} . \tag{19}$$

Eliminating L/L_0 from Eqs. (18) and (19), we arrive at the simple relation

$$[-\chi_E(V)]^{1/3} = (-\chi_0 V^{-2})^{1/3} \tilde{A}^{-1} \, A(V) . \tag{20}$$

Figure 10 demonstrates that the simulation data show the scaling behavior (20) in the entire stability region of the microemulsion. The small deviations from the linear behavior for large areas (i.e., weak amphiphiles) are due to a systematic error of the area calculation for small-scale bicontinuous structures, as discussed in Appendix B.

From the slope of the straight line in Fig. 10 we obtain $(-\chi_0)^{1/3}/\tilde{A} \approx 0.56$. This value characterizes the structure of the microemulsion within an elementary unit. It can be compared with the value of $(-\chi_0)^{1/3}/\tilde{A}$ for *ordered* bicontinuous minimal surfaces (i.e., surfaces with zero mean curvature) [33]. One finds $(-\chi_0)^{1/3}/\tilde{A} \approx 0.680$ for the Schwarz P surface, 0.657 for the D surface, and values in the range 0.66–0.72 for more complicated structures. The deviation of our result from these values can be explained by an increase of area due to thermal fluctu-

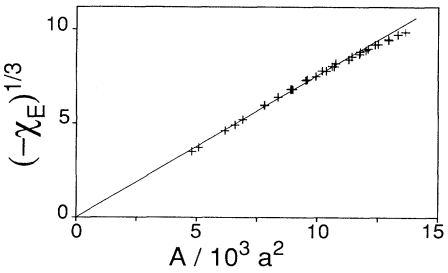

FIG. 10. Scaling relation (20) for internal area A and Euler characteristic χ_E. Data are taken from the entire region of stability of the microemulsion. The deviations for a large area are due to a systematic error of the area calculation algorithm (see Appendix B).

ations and a small number of micelles with positive Euler number and negligible area. Thus, our microemulsion is best characterized as a fluid "plumber's nightmare" phase, with the interfaces forming an irregular "minimal" surface.

V. THE LAMELLAR PHASE

The amphiphilic monolayers in the lamellar phase show strong undulations due to thermal fluctuations. A typical Monte Carlo configuration [of the $\Phi(\mathbf{r}) = 0$ surface] is shown in Fig. 11. These fluctuations have been studied intensively within the curvature model (11) for membranes [4]. In the lamellar phase, the fluctuations $u(\mathbf{x})$ are restricted due to the presence of other membranes, so that $\langle u^2 \rangle = \mu_0 d^2$, where d is the distance between membranes, and μ_0 of order 1 is a constant. For $\sigma = 0$, this leads to an entropic repulsion, which decreases as d^{-2} for large membrane separations [5, 34].

In the simulations of our Ginzburg-Landau model, the

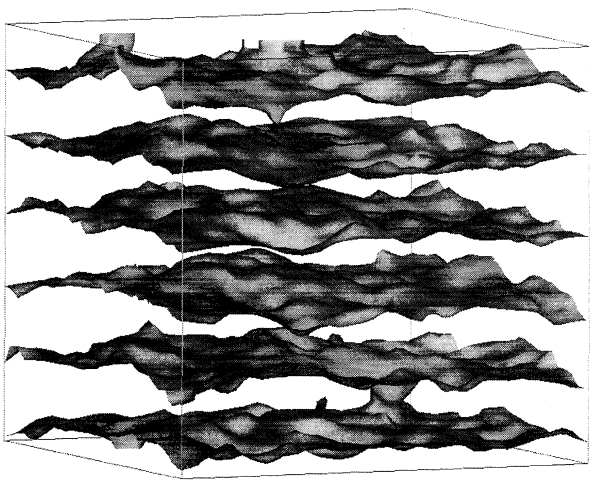

FIG. 11. Typical equilibrium configuration in the lamellar phase at $g_0 = -2.5, f_0 = 0.78$. Shown are only the $\Phi(\mathbf{r}) = 0$ surfaces. Note that there is a passage between the two lowest layers. (The structures at the upper face of the cube are artifacts of the visualization program.)

free energy cannot be calculated easily. Thus, to study the effect of fluctuations in the lamellar phase, we focus on the increase of the internal area due to fluctuations. This is a quantity, which is accessible to experiment, and has been measured recently [35].

A. Excess area

When the fluctuations of the monolayers are neglected, the internal area of the lamellar phase is obtained from a simple geometrical relation, $A = Vd^{-1}$. When the fluctuations are included, the internal area will be somewhat larger than the projected area. The excess area depends on the separation of the membranes. For small undulations, the excess area is [15]

$$\left\langle \frac{A_{\rm real} - A_{\rm proj}}{A_{\rm proj}} \right\rangle = \tfrac{1}{2} \left\langle |\nabla u|^2 \right\rangle = \tfrac{1}{2} \int \frac{d^2q}{(2\pi)^2} \, q^2 \left\langle |\tilde{u}(q)|^2 \right\rangle . \tag{21}$$

Using the equipartition theorem,

$$(\sigma q^2 + \kappa q^4) \left\langle |\tilde{u}(q)|^2 \right\rangle = k_B T , \tag{22}$$

we find

$$\frac{\Delta A}{A} = \frac{k_B T}{8\pi\kappa} \ln \frac{\sigma/\kappa + q_{\rm max}^2}{\sigma/\kappa + q_{\rm min}^2} . \tag{23}$$

Here, the high momentum cutoff $q_{\rm max}$ is determined by the intrinsic width of the oil-water interface,

$$q_{\rm max} = \alpha \frac{2\pi}{\xi_{\rm kink}}, \tag{24}$$

with a constant $\alpha = O(1)$. The low momentum cutoff is $q_{\rm min} = 2\pi/\xi_{\parallel}$, where $\xi_{\parallel}$ is the parallel correlation length. It is determined by the requirement $\langle u^2 \rangle = \mu_0 d^2$,

$$\mu_0 d^2 = \int_{q_{\rm min}}^{q_{\rm max}} \frac{d^2q}{(2\pi)^2} \frac{k_B T}{\sigma q^2 + \kappa q^4} . \tag{25}$$

In the limit $\sigma \to 0$, one finds [36]

$$q_{\rm min} = \sqrt{\frac{k_B T}{4\pi\kappa\mu_0}} \frac{1}{d} . \tag{26}$$

The exact value of μ_0 is not known. For a single membrane between two walls, $\mu_0 \simeq \frac{1}{6}$ [5, 37]. For the bending rigidity κ we use the mean-field results [24] (see Appendix A for details). We want to emphasize that the unrenormalized bending rigidity has to be used in the result (23) for the excess area [15].

Finally we have to take into account that the distance d, which appears in the expressions (25), (26) for the excess area, is the spacing available for the fluctuations of a membrane. Therefore, the width of a single interface has to be subtraced from the periodicity length of the lamellar phase,

$$d = \frac{L}{n} - 2\xi_{\rm kink} , \tag{27}$$

where n is the number of interfaces in a system of length L. Putting everything together, we obtain in the case $\sigma = 0$ the excess area

$$\frac{\Delta A}{A} = \frac{k_B T}{4\pi\kappa} \ln\left(\frac{\sqrt{4\pi\kappa\mu_0}}{\xi_{\text{kink}}}\,\alpha d\right) . \tag{28}$$

This logarithmic behavior of the excess area with membrane separation has been confirmed experimentally [35] for strongly swollen lamellar phases.

In the Monte Carlo simulations, we have used a system of linear size $N = 45$ to determine the excess area, in order to avoid finite-size effects in the direction parallel to the membranes, and simultaneously to allow as many different numbers of layers as possible. It is discussed in Appendix B that we can determine the excess area in the simulations very precisely. We have usually used 50 000 MCS to calculate the averages, so that the statistical error of the averaged excess area is of the order of a few percent. We have studied the excess area at several points in the phase diagram, all of them in the vicinity of the four-phase point [38]. Only in this region of the phase diagram is the lamellar spacing large enough, and the bending rigidity small enough, that the interfacial area is appreciably enlarged by the undulations.

Due to the finite system size, we cannot reach the limit where all other length scales are small compared to the interface separation in the simulations. Furthermore, we have shown in Ref. [7] that the interfacial tension σ only vanishes for the equilibrium distance of the lamellar phase; however, due to the finite system size, this optimal distance usually cannot be reached. For all other separations, exponential corrections to the interfacial tension [7, 14] have to be taken into account,

$$\sigma = \sigma_\infty + \overline{\sigma} e^{-d/\xi_{\text{bulk}}} , \tag{29}$$

where σ_∞ is the renormalized interfacial tension calculated in Sec. III A. We determine the bulk correlation length ξ_{bulk} from a simulation in the pure water phase; at $g_0 = -2.25$, $f_0 = 1.125$ we find $\xi_{\text{bulk}} = 0.759$, somewhat larger than the value obtained from the Ornstein-Zernike approximation. The correction amplitude $\overline{\sigma}$ can be calculated from the spectrum of Gaussian fluctuations of a membrane between walls [7]. We expect $\overline{\sigma} \approx 10$–$20$ from this calculation.

The excess area for a point in the phase diagram near the four-phase point is shown in Fig. 12 as a function of the inverse interface separation $1/d$. The data are compared with the logarithmic behavior (28), which fits the data only over a small interval. However, when the exponential distance dependence of the interfacial tension, Eq. (29), is taken into account in Eq. (23), *all* data can be explained very well. We want to emphasize that this is a fit with almost no free parameters; only α [see Eq. (24)] and $\overline{\sigma}$ are adjustable within narrow boundaries. Thus, the existence of an exponential, d-dependent contribution in the interfacial tension is clearly confirmed by our simulation results.

We can now go further and compare simulation data with the theoretical expectation (23), (29) at different points in the phase diagram. At each point, ξ_{kink}, κ, and σ_∞ have been determined independently. However, identical values of α and $\overline{\sigma}$ are used in all theoretical expressions for the excess area. Five sets of data points in the range $-2.125 < g_0 < -2.375$ and $1.06 < f_0 < 1.125$ are shown in Fig. 13. The scatter of the data is found to be less than 10%.

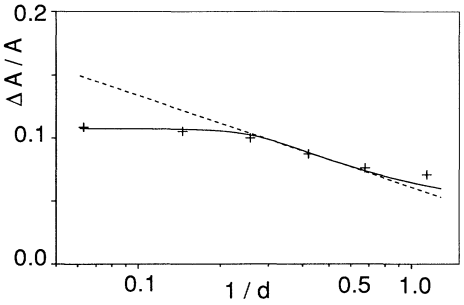

FIG. 12. Excess area in the lamellar phase at $g_0 = -2.25$, $f_0 = 1.125$ for various monolayer separations. Error bars are of the order of the symbol size. The dashed line is the theoretical prediction with $\sigma = 0$; the solid line is obtained from (29) with $\sigma_\infty = 0.25$. The parameters $\mu_0 = 0.16$, $\overline{\sigma} = 12$, and $\alpha = 1.6$ are used in Eqs. (23) and (29).

B. Scattering intensity

The thermal fluctuations of a stack of membranes are most easily studied experimentally by x-ray and neutron scattering. Thus, we want to calculate the scattering intensity from the Monte Carlo simulations. We have shown in Ref. [7] that the scattering intensity of a small number of interfaces between two walls, at any point in the phase diagram where the lamellar phase is stable, strongly depends on the number of interfaces and their separation. In the simulations it turns out to be much easier to compare the scattering intensities of a fixed number of membranes with fixed intermembrane distance

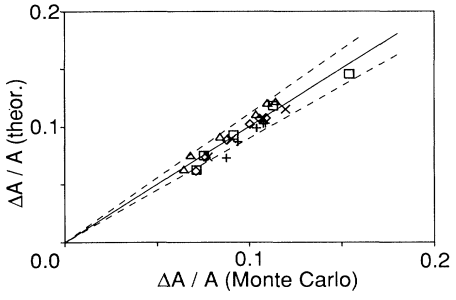

FIG. 13. Comparison of Monte Carlo data and theoretical predictions of excess area for five different points in the phase diagram. Dashed lines indicate a deviation of ±10%. The parameters μ_0, $\overline{\sigma}$, and α are the same as in Fig. 12. $(g_0, f_0) = (-2.375, 1.06)$ (□); $(-2.375, 1.1)$ (△); $(-2.3, 1.09)$ (×); $(-2.25, 1.125)$ (◇); $(-2.125, 1.125)$ (+). The corresponding values of σ_∞ are 0.02, 0.10, 0.14, 0.25, and 0.35 (in the same order).

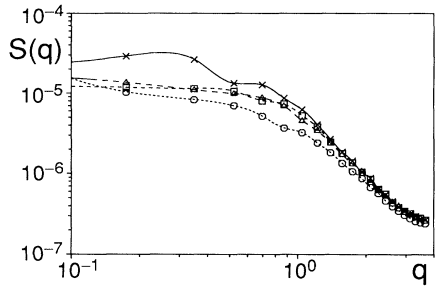

FIG. 14. Scattering intensity for wave vector q parallel to a lamellar stack of six monolayers, for a system with $N = 45$. Parameters are $(g_0, f_0) = (-2.5, 1.125)$, $(-2.5, 1.0)$, $(-2.375, 1.06)$, $(-2.25, 1.125)$ (from above).

at different points in the phase diagram. In this case, the optimal lamellar spacing varies, so that at some points in the phase diagram the stack is effectively depressed, while it is compressed at others. In the first case, the interfacial tension is negative, which leads to a peak at nonzero wave vector q in the scattering intensity; in the latter case the interfacial tension is positive, which implies a peak at $q = 0$. The data presented in Fig. 14 indeed show the expected behavior. Note that the scattering intensity shows several maxima and shoulders at wave vectors $q \simeq 0.3$, 0.7, and 1.0. In the Gaussian approximation [7], these maxima are due to undulation modes, for which neighboring membranes fluctuate opposite to each other.

The behavior of the scattering intensity for large q seems to follow a power-law decay, but has not yet reached the asymptotic q^{-4} behavior, which is expected from the analysis of the Gaussian fluctuations [7]. The upward trend at very large q is due to the periodic boundary conditions.

VI. SUMMARY AND CONCLUSIONS

Fluctuations of oil-water-surfactant mixtures have been studied in a Ginzburg-Landau model by Monte Carlo methods. In order to apply the Monte Carlo method to a continuum-field theory, a background lattice has to be introduced. However, since the lattice constant can be chosen to be much smaller than all other typical length scales of the system, lattice effects can be effectively avoided in our simulations.

The fluctuations alter the phase diagram quantitatively, as compared to the mean-field approximation. The region of stability of the microemulsion increases, both towards oil-rich and water-rich phases, and towards the lamellar phase. The region of stability of the lamellar phase also increases towards oil-rich and water-rich phases. The topology of the *microemulsion* can be characterized by the Euler characteristic χ_E, which measures the connectivity of the surfactant film. The large negative value found in the simulations indicates a structure with many handles. Furthermore, we have shown that a "universal" ratio, $(-\chi_E)^{1/3}V^{2/3}A^{-1}$, can be derived for a system with volume V and internal area A, which quantifies the internal structure of the microemulsion. By comparing the value obtained from the simulations with the known value for ordered bicontinuous phases, we found that to view the microemulsion as a disordered "minimal" surface is very appropriate. Finally, we have determined the increase of the internal area in the *lamellar phase* with increasing distance between lamelli. The results are consistent with the predictions obtained from the curvature model of Helfrich *if* a distance-dependent contribution to the interfacial tension is taken into account. Thus, we have shown that the curvature Hamiltonian is contained as a limiting case in our Ginzburg-Landau theory.

ACKNOWLEDGMENTS

Helpful discussions with K. Mecke are gratefully acknowledged. We thank R. Albrecht from the MPI für Biochemie, Abt. Gerisch, Martinsried, for his help with the visualization of three-dimensional configurations. This work was supported in part by the Deutsche Forschungsgemeinschaft through Sonderforschungsbereich 266.

APPENDIX A: THE OIL-WATER INTERFACE

The Euler-Lagrange equations for the order-parameter profile of inhomogeneous structures in the mean-field approximation can be solved exactly only for special cases [39] or for a piecewise parabolic (constant) approximation to f (g) [16]. To calculate the profile of an interface between homogeneous oil-water phases in the model (1),(2), we use the ansatz

$$\Phi(z) = \Phi_{\rm bulk} \tanh(z/\xi_{\rm kink}) \tag{A1}$$

and minimize the free energy with respect to the interfacial width $\xi_{\rm kink}$. This yields

$$\xi_{\rm kink} = \left[-\frac{5g_0 + g_2}{24} + \sqrt{\left(\frac{5g_0 + g_2}{24}\right)^2 + \frac{1 + 5f_0}{12}} \right]^{-1/2}. \tag{A2}$$

The elastic constants of the interface have been calculated in Ref. [40] under the assumption that the interfacial profile remains unchanged when the interface is bent,

$$\sigma = \int_{-\infty}^{\infty} dz\, [2g(\Phi)(\nabla\Phi)^2 + 4c(\Delta\Phi)^2] \equiv \int_{-\infty}^{\infty} dz\, p_s(z), \tag{A3}$$

$$\kappa = 2c \int_{-\infty}^{\infty} dz (\Phi'(z))^2, \tag{A4}$$

$$\bar{\kappa} = \int_{-\infty}^{\infty} dz\, z^2\, p_s(z) - 2\kappa. \tag{A5}$$

Evaluating these expressions for approximation (A1), we find

$$\sigma = \tfrac{8}{3}\xi_{\rm kink}^{-1} g_0 + \tfrac{8}{15}\xi_{\rm kink}^{-1} g_2 + \tfrac{64}{15}\xi_{\rm kink}^{-3} c, \quad \text{(A6)}$$

$$\kappa = \tfrac{8}{3}\xi_{\rm kink}^{-1} c, \quad \text{(A7)}$$

$$\bar{\kappa} + 2\kappa = g_0 \xi_{\rm kink}(\tfrac{2}{9}\pi^2 - \tfrac{4}{3}) + \tfrac{2}{45}\pi^2(g_2 \xi_{\rm kink} + 8c\xi_{\rm kink}^{-1}) \, . \quad \text{(A8)}$$

The ansatz (A1) for the interfacial profile gives a line of vanishing interfacial free energy, which agrees very well with the exact line of phase transitions from the oil-water phase to the lamellar phase in mean-field theory [20]. Thus, we expect this ansatz also to give good results for the bending moduli κ and $\bar{\kappa}$.

APPENDIX B: CALCULATION OF INTERFACE AREA

The $\Phi(\mathbf{r}) = 0$ surfaces in the lamellar and microemulsion phases can be interpreted as an internal interface between oil and water domains. Its area is an extensive quantity that is enlarged by fluctuations. In the simulations we have continuous values of the order parameter Φ on a cubic lattice. To determine the position of the interface, we interpolate linearly between neighboring lattice sites with a different sign of the order parameter, to obtain the $\Phi = 0$ points on the bonds. These points are then connected by a triangulated surface. With a lattice constant a smaller than all relevant length scales, pathological configurations, i.e., configurations which do not allow a unique choice of the triangulated surface, occur with low probability.

To implement this calculation efficiently, we reduced the number of cases by dividing each unit cell of the lattice into eight subcells. There are six different classes of elementary subcells, with one or two triangles in each subcell. From these triangles, the whole surface can be constructed by sequentially investigating all unit cells of the lattice.

The performance of the algorithm has been tested by calculating the surface of cylindrical and spherical order-parameter distributions. The error is lower than -1% for the relevant radii of curvature, i.e., $3a < r < 8a$ for spheres, and $2a < r$ for cylinders. The area of the bicontinuous simple cubic Schwarz P surface (see, e.g., Ref. [33]) was overestimated by about $+1.5\%$ for unit-cell size $L_0 \geq 9a$, while the error increased to $+4.85\%$ for $L_0 = 5.4a$.

[1] *Physics of Amphiphilic Layers*, edited by J. Meunier, D. Langevin, and N. Boccara, Springer Proceedings in Physics Vol. 21 (Springer, Berlin, 1987); *The Structure and Conformation of Amphiphilic Membranes*, edited by R. Lipowsky, D. Richter, and K. Kremer (Springer, Berlin, 1992); *Modern Ideas and Problems in Amphiphilic Science*, edited by W.M. Gelbart, D. Roux, and A. Ben-Shaul (Springer, Berlin, in press).

[2] L.E. Scriven, Nature **263**, 123 (1976); in *Micellization, Solubilization, and Microemulsions*, edited by K.L. Mittal (Plenum, New York, 1977).

[3] P. Guéring and B. Lindman, Langmuir **1**, 464 (1985); M. Moha-Ouchane, J. Peyrelasse, and C. Boned, Phys. Rev. A **35**, 3027 (1987).

[4] W. Helfrich, Z. Naturforsch. **28c**, 693 (1973).

[5] W. Helfrich, Z. Naturforsch. **33a**, 305 (1978).

[6] P.G. de Gennes and C. Taupin, J. Phys. Chem. **86**, 2294 (1982).

[7] G. Gompper and M. Kraus, preceding paper, Phys. Rev. E **47**, 4289 (1993).

[8] Lattice models of amphiphilic systems are reviewed in G. Gompper and M. Schick, in *Modern Ideas and Problems in Amphiphilic Science*, edited by W.M. Gelbart, D. Roux, and A. Ben-Shaul (Springer, Berlin, in press).

[9] N. Jan and D. Stauffer, J. Phys. (Paris) **49**, 623 (1988); K.A. Dawson, B.L. Walker, and A. Berera, Physica A **165**, 320 (1990).

[10] R.G. Larson, J. Chem. Phys. **91**, 2479 (1989); **96**, 7904 (1992).

[11] M. Laradji, H. Guo, M. Grant, and M.J. Zuckermann, Phys. Rev. A **44**, 8184 (1991); P.A. Slotte, *ibid.* **46**, 6469 (1992).

[12] G. Gompper and M. Schick, Phys. Rev. A **42**, 2137 (1990).

[13] Two other continuum models for ternary fluid mixtures have been considered: B. Smit, A.J. Hilbers, K. Esselink, A.M. Rupert, N.M. van Os, and A.G. Schlijpers, Nature **348**, 624 (1990); J. Phys. Chem. **95**, 6361 (1991) have studied a system of point particles interacting by Lennard-Jones potentials by a molecular-dynamics simulation; T. Kawakatsu and K. Kawasaki, Physica A **167**, 690 (1990) use a hybrid model, where only the amphiphiles are point particles.

[14] M.E. Fisher and A. Jin, Phys. Rev. Lett. **69**, 792 (1992).

[15] W. Helfrich, J. Phys. (Paris) **46**, 1263 (1985).

[16] G. Gompper and M. Schick, Phys. Rev. Lett. **65**, 1116 (1990).

[17] K. Chen, C. Jayaprakash, R. Pandit, and W. Wenzel, Phys. Rev. Lett. **65**, 2736 (1990).

[18] M. Teubner and R. Strey, J. Chem. Phys. **87**, 3195 (1987).

[19] This follows from the behavior of the scattering peak as a function of g_0 (see Ref. [18]), as well as from the wetting behavior (see Ref. [16]).

[20] G. Gompper and S. Zschocke, Phys. Rev. A **46**, 4836 (1992).

[21] F. Brochard and J.F. Lennon, J. Phys. (Paris) **36**, 1035 (1975).

[22] M.P. Gelfand and M.E. Fisher, Physica A **166**, 1 (1990).

[23] L. Peliti and S. Leibler, Phys. Rev. Lett. **54**, 1690 (1985).

[24] Since k_BT is absorbed in the functions c, f, and g of the Ginzburg-Landau model, our results for κ are in units of the thermal energy k_BT.

[25] S.A. Brazovskii, Zh. Eksp. Teor. Fiz. **68**, 175 (1975) [Sov. Phys. JETP **41**, 85 (1975)].

[26] The concept of Euler characteristic is discussed in many textbooks, e.g., M. Nakahara, *Geometry, Topology and Physics* (Hilger, Bristol, 1990).

[27] K. Mecke, Ph.D. thesis, Universität München, 1993 (unpublished).

[28] R. Lipowsky and S. Leibler, Phys. Rev. Lett. **56**, 2541 (1986).
[29] W. Jahn and R. Strey, J. Chem. Phys. **92**, 2294 (1988).
[30] The fluctuation effects on the scattering intensity in a similar model have been studied by renormalization-group methods by Y. Levin, C.J. Mundy, and K.A. Dawson, Phys. Rev. A **45**, 7309 (1992).
[31] S.-H. Chen, S.-L. Chang, and R. Strey, J. Chem. Phys. **93**, 1907 (1990); J. Appl. Cryst. **24**, 72 (1991).
[32] B. Widom, J. Chem. Phys. **90**, 2437 (1989).
[33] D.M. Anderson, H.T. Davis, L.E. Scriven, and J.C.C. Nitsche, Adv. Chem. Phys. **77**, 337 (1990).
[34] C.R. Safinya, D. Roux, G.S. Smith, S.K. Sinha, P. Dimon, N.A. Clark, and A.M. Bellocq, Phys. Rev. Lett. **57**, 2718 (1986); D. Roux and C.R. Safinya, J. Phys. (Paris) **49**, 307 (1988).
[35] R. Strey, R. Schomäcker, D. Roux, F. Nallet, and U. Olsson, J. Chem. Soc. Faraday Trans. **86**, 2253 (1990); D. Roux, F. Nallet, E. Freyssingeas, G. Porte, P. Bassereau, M. Skouri, and J. Marignan, Europhys. Lett. **17**, 575 (1992).
[36] We have tested that this expression remains a good approximation even for the case of small, but nonvanishing σ, as discussed below.
[37] G. Gompper and D.M. Kroll, Europhys. Lett. **9**, 59 (1989); **15**, 783 (1991).
[38] The exact position of the four-phase point is not known exactly. Therefore, some of our simulation data may actually be taken in a region of parameter space, where the lamellar phase is metastable. However, for distance dependence of the excess area studied here, a stable and a metastable lamellar phase should show exactly the same behavior.
[39] G. Gompper, R. Hołyst, and M. Schick, Phys. Rev. A **43**, 3157 (1991).
[40] G. Gompper and S. Zschocke, Europhys. Lett. **16**, 731 (1991).

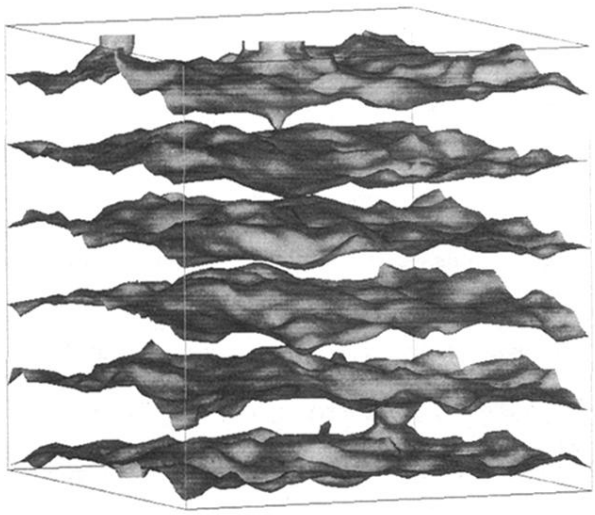

FIG. 11. Typical equilibrium configuration in the lamellar phase at $g_0 = -2.5, f_0 = 0.78$. Shown are only the $\Phi(\mathbf{r}) = 0$ surfaces. Note that there is a passage between the two lowest layers. (The structures at the upper face of the cube are artifacts of the visualization program.)

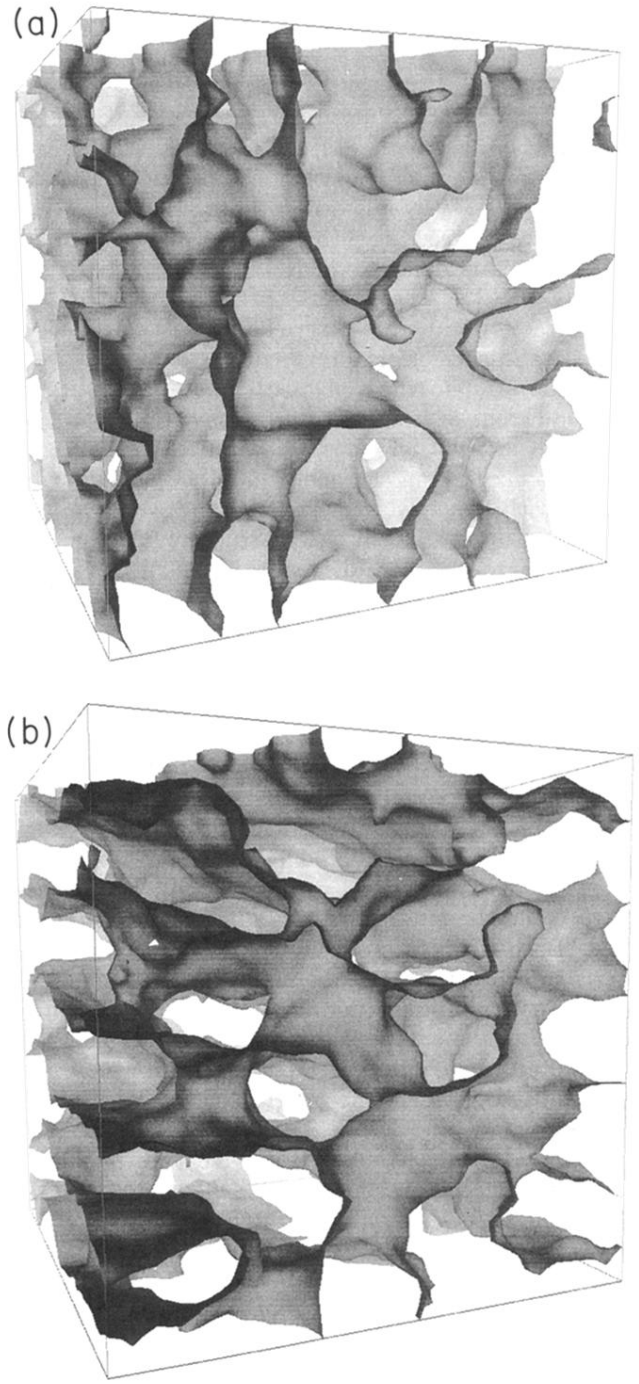

FIG. 7. Typical equilibrium configurations in the microemulsion in the vicinity of the transition to the lamellar phase at (a) $g_0 = -2.5, f_0 = 0.675$ and (b) $g_0 = -2.5, f_0 = 0.695$. Shown are only the $\Phi(\mathbf{r}) = 0$ surfaces. It can be seen that (b) is closer to the transition line, and shows already a local lamellar structure.